IEEE Access
Multidisciplinary ⋮ Rapid Review ⋮ Open Access Journal

Received 15 September 2023, accepted 25 September 2023, date of publication 29 September 2023,
date of current version 13 October 2023.

Digital Object Identifier 10.1109/ACCESS.2023.3320707

RESEARCH ARTICLE

Attitude Estimation of Quadrotor UAV Based on QUKF

TAO LIANG[1], KAILAI YANG[2], QIANG HAN[1,3], CHENJIE LI[1], JUNLIN LI[1], QINGWEN DENG[1], SHIDONG CHEN[1,3], AND XIANGUO TUO[1,3]

[1]School of Automation and Information Engineering, Sichuan University of Science and Engineering, Yibin 644005, China
[2]School of Mechanical Engineering, Sichuan University of Science and Engineering, Yibin 644005, China
[3]Artificial Intelligence Key Laboratory of Sichuan Province, Sichuan University of Science and Engineering, Yibin 644005, China

Corresponding author: Qiang Han (hanqiang1117@163.com)

This work was supported in part by the China University Innovation Fund "New Generation Information Technology Innovation Project" under Grant 2021ITA10002, in part by the Sichuan Province Science and Technology Department Key Research and Development Project under Grant 2021YFG0056, in part by the Sanjiang New District of Yibin City through the Sichuan Province Unveiled the "AM-OLED LCD Device Assembly Bonding Technology Research and Development" under Grant 2022JBGS001, and in part by the Postgraduate Innovation Fund Project of Sichuan University of Science and Engineering under Grant Y2022110.

ABSTRACT Toward the quadcopter unmanned aerial vehicle (UAV) attitude measurement problem, to improve the accuracy of acquisition of vehicle attitude parameters, and ensure accuracy of subsequent attitude control, the Quaternion-based Unscented Kalman filter (QUKF) data fusion method is presented. This attitude measurement system uses STM32F103 as the central controller, MPU6050 with integrated accelerometer and gyroscope, and magnetometer HMC5883l as the measurement sensor. Coordinate Rotation Relationships for the Attitude Heading Reference System (AHRS) in Quaternions, combining Unscented Kalman Filter (UKF) to Fuse Low-Cost Attitude Measurement Systems, tracking estimation of the genuine attitude of the vehicle. High-precision sensor measurements as real values, by comparing with Extended Kalman Filter (EKF), Complementary Filter (CF), and genuine values to validate and analyze the effectiveness of the algorithm applied to the low-cost attitude measurement system. Experimental results show that the low-cost attitude measurement system using quaternions as state variables combined with UKF can accurately estimate attitude information, providing precise attitude information for subsequent attitude control of UAVs.

INDEX TERMS Unscented Kalman filter, quaternion, quadrotor UAV, attitude estimation, data fusion.

I. INTRODUCTION

For the past few years, UAVs have a bright future ahead of them, widely used in both military and civilian applications. Quadcopter UAVs are simple and inexpensive, and they can replace human labor for particular tasks, so a large number of researchers and companies have conducted extensive research in related areas. In quadrotor attitude control, it is crucial to obtain highly accurate and stable attitude information [1], it determines the accuracy of the subsequent attitude control. High-precision attitude sensors can acquire vehicle attitude information. However, high-precision attitude sensors are generally characterized by high cost, bulky and heavy. Currently, quadcopter drones on the market generally consider the cost, load capacity, and other reasons, choosing low-cost, low-precision sensors. And this kind of sensor is susceptible to geomagnetic fields, noise, vibration, and other environmental disturbances; in this case, the accuracy of attitude information acquired by low-precision sensors decreases; it affects the vehicle's stability. Therefore, it is essential to have a stable and highly accurate attitude estimation for the attitude measurement system.

The low-cost MEMS inertial sensors currently available on the market generally include gyroscopes, accelerometers, magnetometers. Gyroscopes in inertial sensors are used for three-axis directional angular velocity measurements, with better dynamic correspondence and accuracy. Still, it exists integral error, long time cumulative error will be enlarged,

The associate editor coordinating the review of this manuscript and approving it for publication was Angel F. García-Fernández.

the stability is relatively poor, and the angle information integrated by the gyroscope is relative to the relative position of the starting point, so it does not provide absolute angle [2]. Accelerometers for measuring acceleration in three axes, with good static performance, but is susceptible to motion acceleration and has lower dynamic accuracy [3]. Magnetometers are used to measure the strength of the magnetic field in the triaxial direction, and external magnetic interference is more sensitive to the magnetic field, easily affected by magnetic fields [4]. Single inertial sensors all have their drawbacks, so they can't be totally trusted, need a fusion algorithm to fuse data from different sensors and estimate valid attitude information.

Noise encountered in UAV attitude measurements is generally filtered using a filtering method to remove the interference caused by the noise [5]. Traditional filtering methods can only be realized when the valid signal and the noise have different frequency bands. In the early 1960s, Kalman [6] and Buse proposed a new linear filtering and prediction theory. This method can process the input and observed signals from noise in a linear state space representation of the equations to find the state of the system or the proper signal, and it was first applied to the design of NASA's Apollo manned lunar landing spacecraft and its navigation system [7]. The typical attitude estimation algorithms are CF [8], Gradient-Descent (GD) method [9], and Kalman filter (KF) [10]. Reference [11] has compared these algorithms, CF and GD are relatively simple and suitable for handling aircraft with limited hardware performance; in the case of hardware satisfaction, KF is the best choice. The KF fusion effect is better than the above two and widely used, but KF can only be applied to some linear systems. For nonlinear systems like UAVs, KF has some limitations [12], but extended some algorithms based on KF have also been derived for nonlinear systems, for example, EKF [13], Particle Filter (PF) [14], and UKF [15]. These filtering methods have higher estimation accuracy compared to CF and GD. PF relies heavily on the estimation of the initial state and has the particle degeneracy problem; UKF is more accurate than EKF and avoids the complex operations of Jacobi matrices for complex nonlinear functions in EKF. Reference [16] has proposed a CF for estimating UAV attitude with small computational effort, however, CF requires high sensor accuracy, and the filtering performance decreases with increasing gyroscope drift error. Reference [17] has proposed KF fusion of gyroscope and accelerometer data to calculate the optimal estimate to correct the output error recursively, but this method does not provide an accurate estimation of the yaw angle and does not apply to nonlinear systems such as UAVs. Reference [18] has applied EKF to multi-axis vehicle attitude estimation, EKF is an expansion of the nonlinear equations into a first-order approximation using Taylor's formula, however, when the linearization assumption does not hold, it leads to a degradation of the filter performance. Reference [19] has utilized an EKF based on the direction cosine matrix for UAV attitude estimation, but nine values in the direction cosine matrix need to be computed, and the amount of computation is more significant compared to the Euler angles and quaternions, which will increase the processor computational load and cannot be tracked in real-time. Reference [20] has proposed an Euler angle-based attitude estimation for UKF multi-rotor UAVs, which improves the accuracy but suffers from gimbal deadlocking.

In this paper, we propose a quaternion-based UKF data fusion method for estimating the flight attitude of a quadrotor under nonlinear state modeling. We use STM32F103 as the core microcontroller, 3-axis gyroscope and 3-axis accelerometer, and 3-axis magnetometer to form a low-cost 9-axis attitude measurement system. Sensor MPU6050 acquires gyroscope/accelerometer raw data information, and sensor HMC5883l obtains magnetometer raw data information. The first step is to calibrate the raw error of each sensor, which is the fixed error of the sensor itself, to improve the accuracy of the input information of the UKF. Updating the state variables of the model using angular velocity information and correction of observations using accelerometer information and magnetometer information. Figure 1 illustrates the attitude measurement system, ω denotes that the gyroscope correction outputs three-axis angular velocity information, a indicates that the accelerometer calibration outputs triaxial acceleration information, m indicates that the magnetometer calibration outputs triaxial magnetic field strength information.

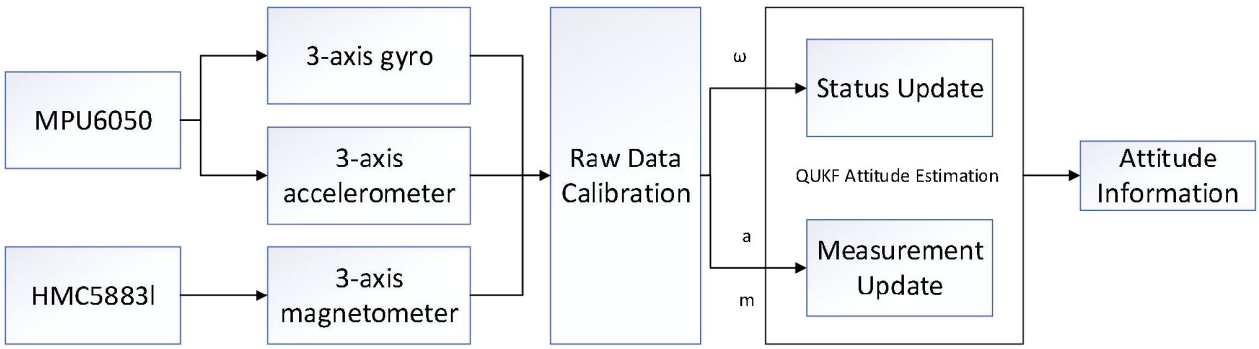

FIGURE 1. The QUKF-based attitude measurement system.

II. MATHEMATICAL MODEL

A. VISION SENSOR

Vehicles generally provide attitude information with a heading attitude reference system (AHRS), this attitude information includes roll angle, pitch angle, and yaw angle. AHRS provides both a navigational coordinate system and an airframe coordinate system, the navigation coordinate system is the reference coordinate system used to solve the attitude information of the aircraft, and in this article, we have chosen the northeastern part of the earth as the navigational coordinate system. The airframe coordinate system is fixed to the vehicle and changes with the movement of the airframe; the x-axis is aligned with the head direction, the y-axis is in the same plane as the body, and in the same direction as the right chord of the body, the z-axis is kept perpendicular to the x-axis and y-axis respectively and pointing down the airframe. As shown in Figure 2.

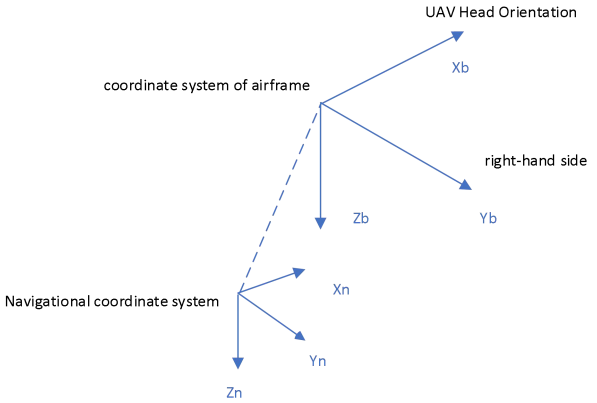

FIGURE 2. Navigation coordinate system and airframe coordinate system.

Expression of the navigation coordinate system in terms of the direction cosine matrix to the airframe coordinate system and the relational formula is built with attitude information, as in: As in (1), shown at the bottom of the page, n represents the navigation coordinate system, b represents the airframe coordinate system, R_n^b represents a rotation from the navigation coordinate system to the airframe coordinate system, ϕ represents rotation of the vehicle around x-axis, the angle of rotation is the roll angle, θ represents the rotation of the vehicle around the y-axis, the angle of rotation is the pitch angle. ψ represents the rotation of the vehicle around the z-axis, and the angle of rotation is the yaw angle. (1) is the rotation matrix expressed in terms of Euler angles, which satisfies $R_b^n = (R_n^b)^T$.

The rotation matrix expressed in terms of Euler angles is straightforward, so the attitude information can be described by the angle of rotation around the three directions. However, it is easy to encounter gimbal lock, so it is easy to produce singular values.

This can be avoided by describing the attitude information in terms of quaternions ($Q = [q_0\ q_1\ q_2\ q_3]^T$), so in this paper, we use quaternions to represent the rotation relation, and the quaternion satisfies the following relation:

$$q_0^2 + q_1^2 + q_2^2 + q_3^2 = 1 \tag{2}$$

$$R_b^n = \begin{bmatrix} q_0^2+q_1^2-q_2^2-q_3^2 & 2(q_1q_2+q_0q_3) & 2(q_1q_3-q_0q_2) \\ 2(q_1q_2-q_0q_3) & q_0^2-q_1^2+q_2^2-q_3^2 & 2(q_2q_3+q_0q_1) \\ 2(q_1q_3+q_0q_2) & 2(q_2q_3-q_0q_1) & q_0^2+q_3^2-q_1^2-q_2^2 \end{bmatrix} \tag{3}$$

As in (3), R_b^n denotes the relational equation for the rotation of the airframe coordinate system to the navigation coordinate system and describes the airframe attitude information in quaternions, again there is the relation $R_n^b = (R_b^n)^T$.

B. CALIBRATION OF SENSOR RAW ERROR

Manufacturers in the production of MPU6050 and HMC5883l such devices, due to process, technology, and other reasons, result in certain defects in the sensor, so in the actual application of the sensor output signal there are specific errors. Therefore, the raw data output from gyroscopes, accelerometers, and magnetometers all have errors, and such errors are deterministic errors, modeling the error calibration:

$$\begin{cases} \omega = R_\omega(\dfrac{\omega'}{c} - \omega_e) \\ a = R_a(\dfrac{a'}{b} - a_e) \\ m = R_m(m' - m_e) \end{cases} \tag{4}$$

As in (4), ω, a, m are the data after calibration of gyroscope, accelerometer and magnetometer respectively; ω', a', m' are gyroscope, accelerometer and magnetometer raw data respectively; ω_e, a_e, m_e are the zero bias error of each sensor; $\frac{\omega'}{c} - \omega_e$, $\frac{a'}{b} - a_e$, $m' - m_e$ compensate for the zero bias error of each sensor, respectively; R_ω, R_a, R_m are the ratios of the maximum and minimum output differences of the sensor in each axial direction, respectively, used to compensate for scale factor errors and axle misalignment of individual sensors; $c = 16.4$ is the ratio of the output range of the MPU6050 data register to the output range of the gyroscope, $b = 1638.35$ is the ratio of the output range of the MPU6050 data register to the output range of the accelerometer.

The gyroscope is placed on a horizontal plane at rest, and by collecting multiple sets of data in each axis, the zero bias in each axis is equal to the average value of the data in that axis;

$$R_n^b = \begin{bmatrix} \cos\theta\cos\psi & \cos\theta\sin\phi\sin\psi - \sin\psi\cos\phi & \cos\theta\sin\phi\cos\psi + \sin\theta\sin\psi \\ \sin\psi\cos\theta & \sin\theta\sin\phi\sin\psi + \cos\phi\cos\psi & \sin\theta\sin\psi\cos\phi - \sin\phi\sin\psi \\ -\sin\theta & \cos\theta\sin\phi & \cos\phi\cos\theta \end{bmatrix} \tag{1}$$

the accelerometer is calibrated using the six-plane calibration method, in which the accelerometer's $\pm X$, $\pm Y$, and $\pm Z$ axes are pointed toward the ground, and the same data are collected in both directions for each axis, and the average value of the data for each axis is calculated; the magnetometer adopts the three-axis rotary table method, in which the magnetometer is fixed on a high-precision three-axis rotary table, and the rotary table is rotated around the X, Y, and Z axes respectively by uniform rotation, and the zero deviation of each axis is equal to the average value of the data in that axis. The calibration parameters for each sensor measured in this paper are as follows:

$$\begin{cases} \omega_e = [1.567 \quad -0.498 \quad -0.787]^T \\ a_e = [0.975 \quad -1.427 \quad -1.977]^T \\ m_e = [0.035 \quad 0.065 \quad 0.075]^T \\ R_\omega = diag(1.005, \quad 0.999, \quad 1.013) \\ R_a = \begin{bmatrix} 1.020 & -0.005 & 0.010 \\ 0.067 & 0.966 & -0.016 \\ 0.008 & -0.014 & 1.080 \end{bmatrix} \\ R_m = diag(1.005 \quad 0.989 \quad 1.012) \end{cases} \tag{5}$$

C. GYROSCOPE-BASED STATE UPDATE

The relationship between quaternions and the angle speed, as in:

$$\dot{Q} = \frac{dQ}{dt} = \frac{1}{2}\Omega(\omega)Q \tag{6}$$

$$\Omega(\omega) = \begin{bmatrix} 0 & -\omega_x & -\omega_y & -\omega_z \\ \omega_x & 0 & \omega_z & -\omega_y \\ \omega_y & -\omega_z & 0 & \omega_x \\ \omega_z & \omega_y & -\omega_x & 0 \end{bmatrix} \tag{7}$$

As in (7), $\omega = [\omega_x \ \omega_y \ \omega_z]$ is the raw data of the gyroscope measurement output after calibration, ω_x, ω_y, ω_z are the angular velocities of rotation about the X, Y, and Z coordinate axes, respectively; $\Omega(\omega)$ denotes the $4 * 4$ opposite matrix. In the discrete equation, the state update belongs to the next moment to the previous moment state value. In each clock cycle T, it is known that the quaternion q_{t-1} and the angular velocity ω_{t-1} at time $t-1$, predictive estimation of the quaternion q_t at time t using $\dot{q}_{t-1}$, as in:

$$q_t = q_{t-1} + T\dot{q}_{t-1} \tag{8}$$

Obtain the state update equation with respect to the quaternion, as in:

$$q_t = q_{t-1} + \frac{T}{2}\Omega(\omega_{t-1})q_{t-1} \tag{9}$$

D. ACCELEROMETER ATTITUDE SOLVING

Accelerometer as an inertial sensor to measure acceleration, the measured output value is the acceleration of three axes in the airframe coordinate system, denoted by $a^b = [a_x^b \ a_y^b \ a_z^b]^T$. According to the measurement principle, when the accelerometer is at rest, it is only subjected to the acceleration of gravity, denoted by $a = [0 \ 0 \ g] = g[0 \ 0 \ 1]$, g ($g = 9.8\text{m/s}^2$) denotes the acceleration of gravity. When the vehicle is in motion, the gravity acceleration information is assigned to three axes according to the attitude angle of the airframe, referring to the (3) we can get:

$$\begin{bmatrix} a_x^b \\ a_y^b \\ a_z^b \end{bmatrix} = R_b^n \begin{bmatrix} 0 \\ 0 \\ g \end{bmatrix} = g \begin{bmatrix} 2(q_1q_3 - q_0q_2) \\ 2(q_2q_3 + q_0q_1) \\ q_0^2 + q_3^2 - q_1^2 - q_2^2 \end{bmatrix} \tag{10}$$

From the three-axis components of the accelerometer output, we can calculate roll angle and pitch angle, as in:

$$\begin{cases} \phi = -\arcsin(\frac{a_x}{g}) \\ \theta = \arctan(\frac{a_y}{a_z}) \end{cases} \tag{11}$$

E. MAGNETOMETER ATTITUDE SOLVING

The magnetometer is used as an inertial sensor to measure the magnetic field strength, and the measured output is the magnetic induction in the three axes of the airframe coordinate system. The magnetometer measurements in the airframe coordinate system are expressed as $m^b = [m_x^b \ m_y^b \ m_z^b]^T$. In the navigational coordinate system, the geomagnetic field always points north along the direction of magnetic induction, has northward and perpendicular components, and no eastward component, so the magnetic field strength is expressed as $m^n = [m_x^n \ m_y^n \ m_z^n]^T$ ($m_y^n = 0$). When the airframe coordinate system coincides with the geomagnetic field in the navigation coordinate system, $M^b = [m_x^n \ 0 \ m_z^n]^T$ is the output of the magnetometer. Since $M^b = m^n$, it satisfies $m^b = R_n^b M^n$, and by rotating it, we realize the conversion between the airframe coordinate system and the navigation coordinate system, and the relationship between the magnetic field strengths of the two coordinate systems is expressed as:

$$\begin{bmatrix} m_x^b \\ m_y^b \\ m_z^b \end{bmatrix} = \begin{bmatrix} m_x^n \cos\theta\cos\psi - m_z^n \sin\theta \\ m_z^n \sin\phi\cos\theta + m_x^n(\sin\phi\cos\theta\cos\psi - \cos\phi\sin\psi) \\ m_z^n \cos\phi\cos\theta + m_x^n(\cos\phi\cos\theta\cos\psi - \sin\phi\sin\psi) \end{bmatrix} \tag{12}$$

Therefore, the component of the magnetic field strength in the horizontal direction is:

$$\begin{cases} m_x^n \sin\psi = m_z^b \sin\phi - m_y^b \cos\phi \\ m_x^n \cos\psi = m_x^b \cos\theta + m_y^b \sin\phi \sin\theta + m_z^b \sin\theta \cos\phi \end{cases} \tag{13}$$

Define the positive yaw angle when the head of the airframe is turned clockwise, the yaw angle can be obtained from (13), as in:

$$\psi = \arctan \frac{m_y^b \cos\phi - m_z^b \sin\phi}{m_x^b \cos\theta + m_y^b \sin\phi \sin\theta + m_z^b \sin\theta \cos\phi} \tag{14}$$

F. QUATERNIONS AND EULER ANGLE CONVERSIONS

A quaternion matrix can be constructed by rotating an axis and the angle of rotation around that axis, as in:

$$\begin{cases} \tilde{q}0 = \cos\frac{\psi}{2}\cos\frac{\theta}{2}\cos\frac{\phi}{2} + \sin\frac{\psi}{2}\sin\frac{\theta}{2}\sin\frac{\phi}{2} \\ \tilde{q}1 = \cos\frac{\psi}{2}\cos\frac{\theta}{2}\sin\frac{\phi}{2} - \sin\frac{\psi}{2}\sin\frac{\theta}{2}\cos\frac{\phi}{2} \\ \tilde{q}2 = \sin\frac{\psi}{2}\cos\frac{\theta}{2}\sin\frac{\phi}{2} + \cos\frac{\psi}{2}\sin\frac{\theta}{2}\cos\frac{\phi}{2} \\ \tilde{q}3 = \sin\frac{\psi}{2}\cos\frac{\theta}{2}\cos\frac{\phi}{2} - \cos\frac{\psi}{2}\sin\frac{\theta}{2}\sin\frac{\phi}{2} \end{cases} \tag{15}$$

As in (15), can be launched $Q = [\tilde{q}0\ \tilde{q}1\ \tilde{q}2\ \tilde{q}3]^T$.

G. SYSTEM EQUATION OF STATE DESIGN

Equation of state and measurement equations for quadrotors:

$$\begin{cases} x_t = f(x,t) + w_t \\ z = h(x,t) + v_t \end{cases} \tag{16}$$

Due to the nonlinear characteristics of the aircraft system, it can be assumed as a discrete nonlinear system with Gaussian noise, as in:

$$\begin{cases} X_{t+1} = F(X,t) + W_t \\ Z_{t+1} = HX(t) + V_t \end{cases} \tag{17}$$

As in (16) and (17), X represents the state vector of the system, Z is denoted as the measured output value of the sensor at time t, The nonlinear functions F and H denote the state transfer matrix, the sensor measurement matrix, respectively; W_t denotes the system noise of the equation of state, V_t denotes the system noise of the measurement equation, and all obey the Gaussian distribution of the noise, $W_t \sim N(0,S)$, $V_t \sim N(0,R)$, S and R denote the covariance matrix of W_t and V_t respectively.

In this paper, we use quaternions as system state variables, that is $X = [q0\ q1\ q2\ q3]^T$. Acceleration and magnetometer solved attitude information as observations in the measurement equation, that is $Z = [\tilde{q}0\ \tilde{q}1\ \tilde{q}2\ \tilde{q}3]^T$. Included among these:

$$F = \left(\begin{bmatrix} 1 & 0 & 0 & 0 \\ 0 & 1 & 0 & 0 \\ 0 & 0 & 1 & 0 \\ 0 & 0 & 0 & 1 \end{bmatrix} + \frac{T}{2}\Omega(\omega) \right) X(t) \tag{18}$$

$$H = \begin{bmatrix} 1 & 0 & 0 & 0 \\ 0 & 1 & 0 & 0 \\ 0 & 0 & 1 & 0 \\ 0 & 0 & 0 & 1 \end{bmatrix} \tag{19}$$

III. ATTITUDE INFORMATION FUSION ALGORITHM DESIGN

Due to the nonlinear characteristics of the discretized equations of state and measurement equations of quadrotors. This paper processes nonlinear equations using UKF, enabling status updates for precise attitude information. The following equations can express the algorithm, as in:

Determine $2n+1$ *Sigma* points at time $t-1$, the sampling points:

$$\begin{cases} \chi_{t-1}^i = \hat{X}_{t-1}, & i = 0 \\ \chi_{t-1}^i = \hat{X}_{t-1} + \sqrt{(n+\lambda)P_{t-1}}, & i = 1 \sim n \\ \chi_{t-1}^i = \hat{X}_{t-1} - \sqrt{(n+\lambda)P_{t-1}}, & i = n+1 \sim 2n \end{cases} \tag{20}$$

Calculate the weights corresponding to the sampling points:

$$\begin{cases} \xi_m^0 = \dfrac{\lambda}{n+\lambda} \\ \xi_c^0 = \dfrac{\lambda}{n+\lambda} + (1-\alpha^2+\beta) \\ \xi_m^i = \xi_c^i = \dfrac{\lambda}{2(n+\lambda)}, i = 1 \sim 2n \end{cases} \tag{21}$$

As in (20) and (21), χ_{t-1}^i is the sampling points in the original state distribution selected by rule such that the mean and covariance of these sampling points are equal to the standard and covariance of the initial state distribution, n is the number of state variables, $\hat{X}_{t-1}$ is the state variable at moment $t-1$, λ is a scaling parameter used to reduce prediction error. P_{t-1} is the error covariance matrix at time $t-1$, α is a parameter controlling the state of the distribution of sampling points.

Substituting the points *Sigma* calculated in (20) into the nonlinear equation of state (17):

$$\chi_{t|t-1}^i = F(\chi_{t-1}^i), \quad i = 0 \sim 2n \tag{22}$$

Calculating one-step prediction and covariance matrices for system state quantities:

$$\hat{X}_{t|t-1} = \sum_{i=0}^{2n} \xi^i \chi_{t|t-1}^i \tag{23}$$

$$P_{t|t-1} = \sum_{i=0}^{2n} \xi^i (\chi_{t|t-1}^i - \hat{X}_{t|t-1})(\chi_{t|t-1}^i - \hat{X}_{t|t-1})^T + Q \tag{24}$$

Based on the one-step prediction values, the UT transformation is used again to produce new set of *Sigma* points:

$$\begin{cases} \tilde{X}_{t|t-1}^i = \hat{X}_{t|t-1}, & i = 0 \\ \tilde{X}_{t-1}^i = \hat{X}_{t|t-1} + \sqrt{(n+\lambda)P_{t|t-1}}, & i = 1 \sim n \\ \tilde{X}_{t-1}^i = \hat{X}_{t|t-1} - \sqrt{(n+\lambda)P_{t|t-1}}, & i = n+1 \sim 2n \end{cases} \tag{25}$$

The predicted *Sigma* points set are brought into the measurement equation to obtain the predicted observations:

$$Z_t^i = H\tilde{X}_{t|t-1}^i, i = 0 \sim 2n \tag{26}$$

The mean of the system prediction and its covariance are obtained by weighted summation:

$$\hat{Z}_t^i = \sum_{i=0}^{2n} \xi^i Z_t^i, i = 0 \sim 2n \tag{27}$$

$$P_{ztzt} = \sum_{i=0}^{2n} \xi^i (Z_t^i - \hat{Z}_i^t)(Z_t^i - \hat{Z}_i^t)^T + R \tag{28}$$

$$P_{xtzt} = \sum_{i=0}^{2n} \xi^i (\tilde{X}_{t|t-1}^i - \hat{Z}_i^t)(Z_t^i - \hat{Z}_i^t)^T \tag{29}$$

Obtain the *kalman* gain matrix:

$$K_t = \frac{P_{xtzt}}{P_{ztzt}} \tag{30}$$

Finally update the state and covariance matrix:

$$\hat{X}_t = \hat{X}_{t|t-1} + K_t(Z_t^i - \hat{Z}_t^i) \tag{31}$$

$$P_t = P_{t|t-1} - K_t P_{zkzk}(K_t)^T \tag{32}$$

IV. EXPERIMENTAL VERIFICATION

In order to verify the effectiveness of the algorithm, we choose a low-cost flight controller for our experiments, STM32F103 as a microcontroller, inertial sensor MPU6050 as a 3-axis gyroscope and 3-axis accelerometer, HMC5883l as a 3-axis magnetometer. We built a Pixhawk-based flight experiment platform and conducted UAV dynamic flight experiments outdoors, as shown in Figure 3. The data collected by the High Precision Sensor MTI-300 is used as the real data, and the data measured by the low-cost sensor is used as the data required for attitude fusion, storing the synchronized collected flight data on the SD card of the flight control board, and set the sampling frequency to 20 HZ, and we select continuous 30s attitude measurement data, finally, data fusion of nine-axis data using Matlab. Comparison and analysis of the data measured by the QUKF proposed in this paper with EKF, CF, and high-precision attitude sensors. In the experiment, according to the stability and accuracy of the algorithm as the dominant conditions, after simulation and debugging to selection the parameters $\lambda = -1$, $\alpha = 1$, $\beta = 2$, $S = diag(0.001, 0.001, 0.001, 0.001)$, $R = diag(0.05, 0.05, 0.05, 0.05)$, in order to ensure the feasibility of the algorithms, different algorithms all use the same noise covariance matrix S and R, and the initial values of the state variables are all set to $X = [1000]^T$.

FIGURE 3. Quadrotor.

Figure 4 represents the calibrated data of the gyroscope, accelerometer, and magnetometer in the hovering condition. Figures 5-7 indicate that the roll angle, pitch angle, and yaw angle estimates of the low-accuracy sensors are compared with the true values by applying different algorithms in the hovering condition. As can be seen from Figure 5, the rollangles estimated by QUKF, EKF, and CF are basically kept around $-0.7°$ and almost straight, and by zooming in, it can be observed that the roll angles fused by the QUKF algorithm are closer to the real values, so the stability of QUKF is more excellent. As can be seen from Figure 6, the pitch angles estimated by the three algorithms are basically kept around $-0.2°$, and by zooming in, it can be observed that both QUKF and EKF are closer to the real value. As can be seen from Figure 7, the yaw angles estimated by the three algorithms are basically kept at 66.7°, by zooming in, it is observed that the QUKF estimates are closer to the real values and have excellent stability. Overall, the estimated attitude angles of the three algorithms are basically consistent with the real values in the hovering condition, and the estimated attitude angles of QUKF are closer to the real values than those of EKF and CF, tolerance is basically within 0.2°,and the stability is also more excellent.

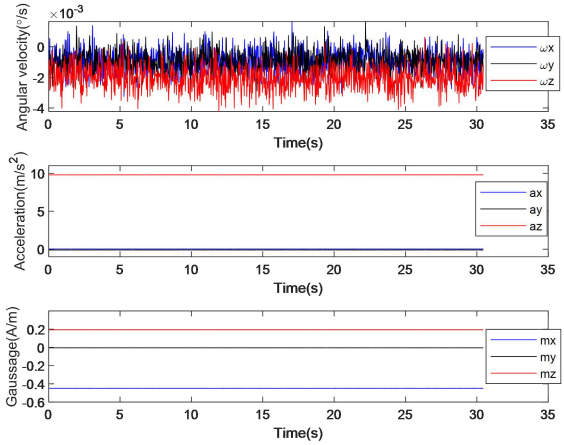

FIGURE 4. Gyroscope, accelerometer, and magnetometer calibrated in hovering state.

Figure 8 represents the data of the gyroscope, accelerometer, and magnetometer after calibration in an outdoor dynamic flight environment. Figures 9-11 represent the comparison of roll angle, pitch angle, yaw angle estimation of the low accuracy sensor with the real values using different algorithms in a motion environment. Based on the comparison, it can be observed that all the three algorithms perform well in attitude estimation and basically track the real attitude angle. By observing 10*s* and 29*s* in Figure 9, it can be observed that the QUKF estimates are much closer to the true values, and the stability of both QUKF and EKF is excellent, while the CF shows a large amount of jitter. By observing 6*s* and 27*s* in Figure 10, It can be observed that

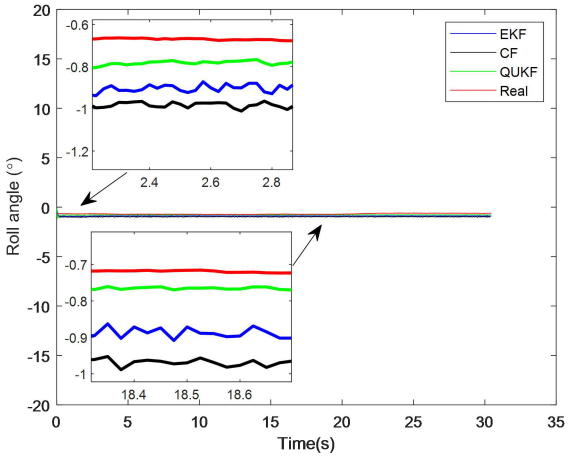

FIGURE 5. Comparison of roll angle in hovering state.

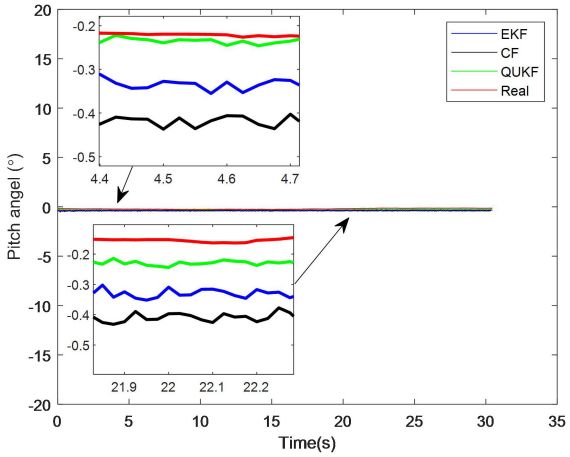

FIGURE 6. Comparison of pitch angle in hovering state.

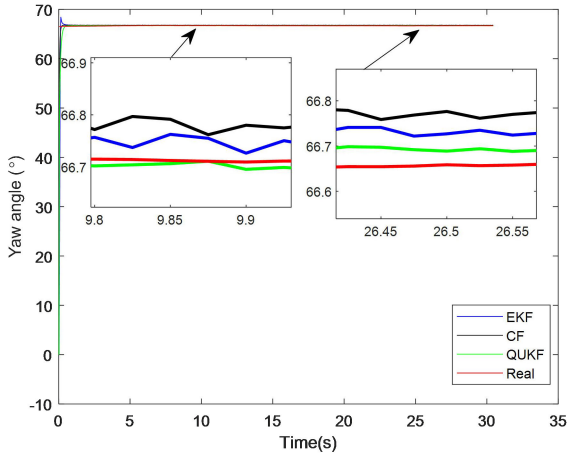

FIGURE 7. Comparison of yaw angle in hovering state.

the QUKF estimates are closer to the true values compared to EKF and CF, and the QUKF and EKF curves are smoother and have better stability compared to CF. By observing 11s and 28s in Figure 11, it can be observed that the QUKF estimates are closer to the true values, and both QUKF and EKF curves are smoother, while CF is more volatile and less stable. Overall, all three algorithms can basically track the real attitude angle in the motion state, and the estimated attitude angle of QUKF is more accurate compared to EKF and CF, and the curves of QUKF and EKF are smoother, and the stability is more excellent compared to CF.

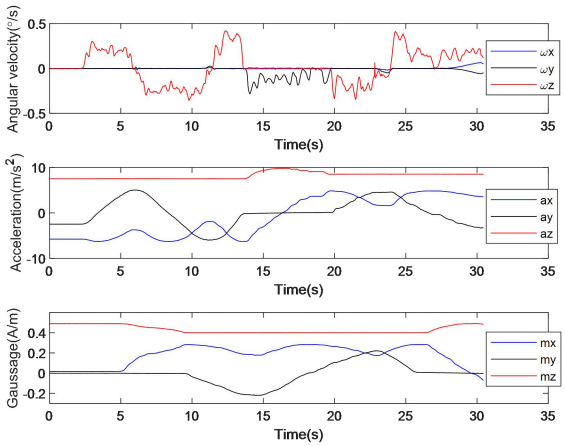

FIGURE 8. Gyroscopes, accelerometers, magnetometers calibrated in motion.

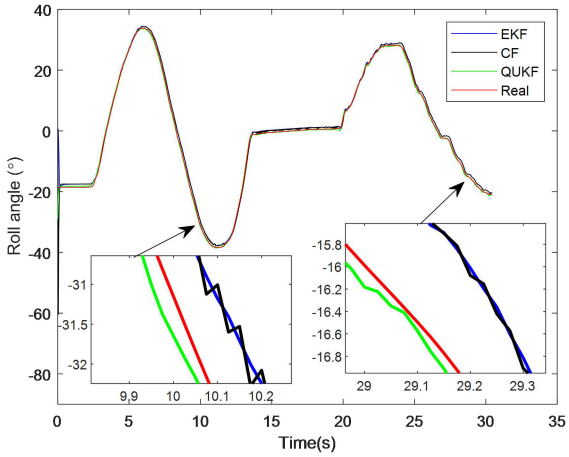

FIGURE 9. Comparison of roll angle under motion.

Comparison of the accuracy of attitude angle estimation using two error analysis metrics, Root Mean Square Error (RMSE) and Mean Absolute Error (MAE), respectively. As shown in table 1:

From the data in the table, the attitude angle errors estimated based on the QUKF are smaller than the latter two, and based on the RMSE, it can be seen that the QUKF has an average decrease of 0.2° compared to the EKF estimation error, and an average decrease of 0.5° compared to the CF estimation error. Overall, the attitude estimation accuracy of QUKF for quadrotor UAVs is higher than that of EKF, CF algorithm.

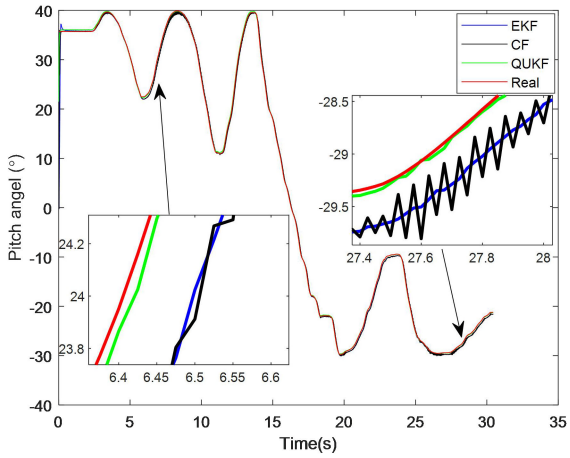

FIGURE 10. Comparison of pitch angle under motion.

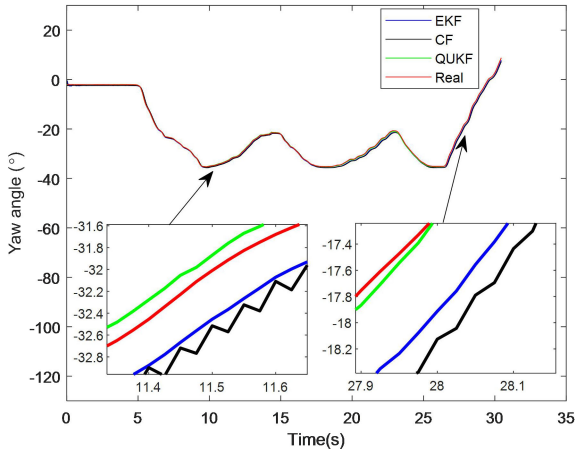

FIGURE 11. Comparison of yaw angle under motion.

TABLE 1. Comparison of RMSE and MAE.

	RMSE			*MAE*		
	roll	*pitch*	*yaw*	*roll*	*pitch*	*yaw*
QUKF	0.5288	0.6891	0.5821	0.3582	0.4224	0.4163
EKF	0.8122	0.8934	0.7526	0.7564	0.6827	0.6135
CF	1.1548	1.0438	1.0745	1.0652	0.8307	0.8677

V. CONCLUDE

In this paper, STM32F103 is used as the controller in hardware, MPU6050 and HMC5883l are used as low-cost sensors. Aiming at the nonlinear characteristics of the flight environment of the aircraft, the QUKF algorithm with higher estimation accuracy is proposed, filtering out Gaussian noise encountered by sensors during vehicle flight by fusing the corrected data from gyroscopes, accelerometers, and magnetometers, determining the attitude angle of the vehicle by attitude solving. Finally, by analyzing and comparing with EKF and CF algorithms, it is concluded that the accuracy of QUKF estimation is higher than that of EKF and CF algorithms, and the robustness is also better, which can effectively improve the accuracy of attitude measurement. Therefore, the attitude angle estimated by the low-precision sensor designed in this paper through the fusion algorithm can be similar to that of the high-precision sensor, which meets the practical requirements of UAV attitude solving.

REFERENCES

[1] F. Jiang, F. Pourpanah, and Q. Hao, "Design, implementation, and evaluation of a neural-network-based quadcopter UAV system," *IEEE Trans. Ind. Electron.*, vol. 67, no. 3, pp. 2076–2085, Mar. 2020, doi: 10.1109/TIE.2019.2905808.

[2] V. M. N. Passaro, A. Cuccovillo, L. Vaiani, M. De Carlo, and C. E. Campanella, "Gyroscope technology and applications: A review in the industrial perspective," *Sensors*, vol. 17, no. 10, p. 2284, Oct. 2017, doi: 10.3390/s17102284.

[3] L. Gao, A. K. Bourke, and J. Nelson, "Evaluation of accelerometer based multi-sensor versus single-sensor activity recognition systems," *Med. Eng. Phys.*, vol. 36, no. 6, pp. 779–785, Jun. 2014, doi: 10.1016/j.medengphy.2014.02.012.

[4] H. A. Hashim, L. J. Brown, and K. McIsaac, "Nonlinear stochastic attitude filters on the special orthogonal group 3: Ito and Stratonovich," *IEEE Trans. Syst., Man, Cybern., Syst.*, vol. 49, no. 9, pp. 1853–1865, Sep. 2019, doi: 10.1109/tsmc.2018.2870290.

[5] F. L. Markley, J. Crassidis, and Y. Cheng, "Nonlinear attitude filtering methods," in *Proc. AIAA Guid., Navigat., Control Conf. Exhibit*, Aug. 2005, p. 5927, doi: 10.2514/6.2005-5927.

[6] G. F. Welch, "Kalman filter," in *Computer Vision: A Reference Guide*, 2020, pp. 1–3, doi: 10.1007/978-3-030-03243-2_716-1.

[7] F. E. Garrett-Bakelman et al., "The NASA twins study: A multidimensional analysis of a year-long human spaceflight," *Science*, vol. 364, no. 6436, Apr. 2019, eaau8650, doi: 10.1126/science.aau8650.

[8] V. Kubelka and M. Reinstein, "Complementary filtering approach to orientation estimation using inertial sensors only," in *Proc. IEEE Int. Conf. Robot. Autom.*, May 2012, pp. 599–605, doi: 10.1109/ICRA.2012.6224564.

[9] M. Petrović, V. Rakočević, N. Kontrec, S. Panić, and D. Ilić, "Hybridization of accelerated gradient descent method," *Numer. Algorithms*, vol. 79, no. 3, pp. 769–786, Nov. 2018, doi: 10.1007/s11075-017-0460-4.

[10] Q. Li, R. Li, K. Ji, and W. Dai, "Kalman filter and its application," in *Proc. 8th Int. Conf. Intell. Netw. Intell. Syst. (ICINIS)*, Nov. 2015, pp. 74–77, doi: 10.1109/ICINIS.2015.35.

[11] N. Koksal, M. Jalalmaab, and B. Fidan, "Adaptive linear quadratic attitude tracking control of a quadrotor UAV based on IMU sensor data fusion," *Sensors*, vol. 19, no. 1, p. 46, Dec. 2018, doi: 10.3390/s19010046.

[12] Y. Zhu, J. Liu, R. Yu, Z. Mu, L. Huang, J. Chen, and J. Chen, "Attitude solving algorithm and FPGA implementation of four-rotor UAV based on improved Mahony complementary filter," *Sensors*, vol. 22, no. 17, p. 6411, Aug. 2022, doi: 10.3390/s22176411.

[13] S. Yang and M. Baum, "Extended Kalman filter for extended object tracking," in *Proc. IEEE Int. Conf. Acoust., Speech Signal Process. (ICASSP)*, Mar. 2017, pp. 4386–4390, doi: 10.1109/ICASSP.2017.7952985.

[14] I. Askari, M. A. Haile, X. Tu, and H. Fang, "Implicit particle filtering via a bank of nonlinear Kalman filters," *Automatica*, vol. 145, Nov. 2022, Art. no. 110469, doi: 10.1016/j.automatica.2022.110469.

[15] S. Antonov, A. Fehn, and A. Kugi, "Unscented Kalman filter for vehicle state estimation," *Vehicle Syst. Dyn.*, vol. 49, no. 9, pp. 1497–1520, Sep. 2011, doi: 10.1080/00423114.2010.527994.

[16] A. Noordin, M. A. M. Basri, and Z. Mohamed, "Sensor fusion algorithm by complementary filter for attitude estimation of quadrotor with low-cost IMU," *TELKOMNIKA, Telecommun. Comput. Electron. Control*, vol. 16, no. 2, pp. 868–875, Apr. 2018, doi: 10.12928/telkomnika.v16i2.9020.

[17] A. Kaba, A. Ermeydan, and E. Kiyak, "Model derivation, attitude control and Kalman filter estimation of a quadcopter," in *Proc. 4th Int. Conf. Electr. Electron. Eng. (ICEEE)*, Apr. 2017, pp. 210–214, doi: 10.1109/ICEEE2.2017.7935821.

[18] S. A. Ludwig and K. D. Burnham, "Comparison of Euler estimate using extended Kalman filter, Madgwick and Mahony on quadcopter flight data," in *Proc. Int. Conf. Unmanned Aircr. Syst. (ICUAS)*, Jun. 2018, pp. 1236–1241, doi: 10.1109/ICUAS.2018.8453465.
[19] J. A. A. S. Somasiri, D. P. Chandima, and A. G. B. P. Jayasekara, "Extended Kalman filter based autonomous flying system for quadcopters," in *Proc. 2nd Int. Conf. Electr. Eng. (EECon)*, Sep. 2018, pp. 130–137, doi: 10.1109/EECon.2018.8541019.
[20] B. Kada, K. Munawar, M. S. Shaikh, M. A. Hussaini, and U. M. Al-Saggaf, "UAV attitude estimation using nonlinear filtering and low-cost MEMS sensors," *IFAC-PapersOnLine*, vol. 49, no. 21, pp. 521–528, 2016, doi: 10.1016/j.ifacol.2016.10.655.

TAO LIANG received the B.S. degree in measurement and control technology and instrumentation from the Sichuan University of Science and Engineering, Yibin, China, in 2020, where he is currently pursuing the M.S. degree. His research interest includes UAV attitude estimation and control.

KAILAI YANG received the B.S. degree in process equipment and control engineering and the M.S. degree in mechanical engineering from the Sichuan University of Science and Engineering, Yibin, China, in 2020 and 2023, respectively. His research interests include the digitalization of intelligent equipment and manufacturing process.

QIANG HAN was born in Shandong, China, in 1987. He received the Ph.D. degree from the Southwest University of Science and Technology, Mianyang, China. He is currently a Lecturer with the Sichuan University of Science and Engineering. His research interests include nonlinear system control, complex networks, and the cooperative control of UAV formation.

CHENJIE LI received the B.S. degree in measurement and control technology and instrumentation from the Sichuan University of Science and Engineering, Yibin, China, in 2021, where he is currently pursuing the M.S. degree. His research interest includes data processing.

JUNLIN LI received the B.S. degree in the Internet of Things engineering from the Sichuan University of Arts and Science, Dazhou, China, in 2020. He is currently pursuing the M.S. degree with the Sichuan University of Science and Engineering, Yibin, China. His research interests include UAV path planning and obstacle avoidance.

QINGWEN DENG received the B.S. degree in electrical engineering and automation from the Sichuan University of Science and Engineering, Yibin, China, in 2022, where he is currently pursuing the M.S. degree. His research interest includes data processing.

SHIDONG CHEN received the B.S. degree in building electrical and intelligent from Yangtze Normal University, Chongqing, China, in 2021. He is currently pursuing the M.S. degree with the Sichuan University of Science and Engineering, Yibin, China. His research interest includes nonlinear system control.

XIANGUO TUO was born in Hunan, China, in 1965. He received the Ph.D. degree from the Chengdu University of Technology, Chengdu, China. He is currently a Professor with the Sichuan University of Science and Engineering. His research interests include nuclear technology theory, nuclear geophysical exploration methods, the development of nuclear electronic instruments, radiation environment assessment, nuclide migration, and environmental monitoring and disaster warning methods.